catalysts

MDPI

Article

In Situ DRIFTS Investigation on CeO_x Catalyst Supported by Fly-Ash-Made Porous Cordierite Ceramics for Low-Temperature NH_3-SCR of NO_X

Shaoxin Wang [1,2], Ziwei Chen [1], Beini He [1], Zheng Yan [3,*], Hao Wang [1,2], Lili Liu [1,2] and Xidong Wang [1,2,*]

1 Department of Energy and Resources Engineering, College of Engineering, Peking University, Beijing 100871, China; wangshaoxin@pku.edu.cn (S.W.); zwchen@pku.edu.cn (Z.C.); hebeini@pku.edu.cn (B.H.); wanghao3352@163.com (H.W.); liu-0806@163.com (L.L.)

2 Beijing Key Laboratory for Solid Waste Utilization and Management, Peking University, Beijing 100871, China

3 College of Energy and Environment, Shenyang Aerospace University, Liaoning 110034, China

* Correspondence: yanzheng@sau.edu.cn (Z.Y.); xidong@pku.edu.cn (X.W.)

Received: 27 March 2019; Accepted: 24 May 2019; Published: 29 May 2019

Abstract: A series of CeO_x catalysts supported by commercial porous cordierite ceramics (CPCC) and synthesized porous cordierite ceramics (SPCC) from fly ash were prepared for selective catalytic reduction of NO_x with ammonia (NH_3-SCR). A greater than 90% NO_x conversion rate was achieved by the SPCC supported catalyst at 250–300 °C when the concentration of loading precursor was 0.6 mol/L (denoted as 0.6Ce/SPCC), which is more advantageous than the CPCC supported ones. The EDS mapping results reveal the existence of evenly distributed impurities on the surface of SPCC, which hence might be able to provide more attachment sites for CeO_x particles. Further measurements with temperature programmed reduction by hydrogen (H_2-TPR) demonstrate more reducible species on the surface of 0.6Ce/SPCC, thus giving rise to better NH_3-SCR performance at a low-temperature range. The X-ray photoelectron spectroscopy (XPS) analyses reveal that the Ce atom ratio is higher in 0.6Ce/SPCC, indicating that a higher concentration of catalytic active sites could be found on the surface of 0.6Ce/SPCC. The in situ diffused reflectance infrared fourier transform spectroscopy (DRIFTS) results indicate that the SCR reactions over 0.6Ce/SPCC follow both Eley-Rideal (E-R) and Langmuir-Hinshelwood (L-H) mechanisms. Hence, the SPCC might be a promising candidate to provide support for NH_3-SCR catalysts, which also provide a valuable approach to recycling the fly ash.

Keywords: in situ DRIFTS; fly ash; cordierite ceramics; NH_3-SCR; CeO_x catalyst; NO_x

1. Introduction

Nitrogen oxides (NO_x) are major air pollutants in ambient air, contributing to the formation of secondary inorganic aerosols, increasing nitrate/sulfate ratios in precipitation and leading to climate forcing effects [1]. Nowadays, it is still a major challenge to purify the NO_x from waste gas effectively [2]. NH_3-SCR has been widely acknowledged as the most efficient method for flue gas denitration in thermal power plants, while an SCR catalyst with high performance and stability is regarded as the core of the SCR technology [3–5]. V_2O_5-WO_3/TiO_2 and V_2O_5-MoO_3/TiO_2 are commercial catalysts that are widely used in treating NO_x from large scale stationary and mobile sources [6,7]. Nevertheless, these commercial catalysts can only show high catalytic efficiency in a narrow temperature window of 300–400 °C, requiring the SCR unit to be placed in the upstream of the electrostatic precipitant and desulfurizer where high concentration of SO_2 and dust are major threats to the catalyst [2,8]. In addition,

the toxicity and relative high expense of V_2O_5 are other shortcomings of these catalysts [3,9]. Thus, many efforts have been devoted to investigation of the fabrication mechanism on low-temperature (<300 °C), as well as environmentally friendly and low-cost SCR catalysts intended for a tail-end SCR configuration [10].

Recently, Ce-containing catalysts have attracted a lot of attention for their superior de-NO_X activities that are caused by their unique oxygen storage properties [11–15]. Cao et al. [16] prepared a CeO_2/TiO_2 catalyst with high SCR activity due to enhanced "fast SCR" reactions following the L-H mechanism. Qu et al. [17] successfully improved the performance of MnO_x-CeO_y/γ-Al_2O_3 in NH_3-SCR of NO by using support modification. Ce-Ti amorphous oxides catalysts for NH_3-SCR with high NO_x conversion ratios were prepared by Li et al. [18], while the SCR activity of pure CeO_2 was rather low across the whole testing temperature range. It has been demonstrated that the catalyst supports play a crucial role in the performance of Ce-containing catalysts. Nonetheless, the aforementioned catalyst supports such as TiO_2 and γ-Al_2O_3 are highly expensive in large scale industrial applications. Therefore, it is significant to find low-cost catalyst supports and make the reaction mechanism clear.

Porous cordierite ($2MgO{\cdot}2Al_2O_3{\cdot}5SiO_2$) ceramics have been widely adopted as catalyst supports due to their high chemical and mechanical stability, low thermal expansion coefficient and high porosity [19]. Qiu et al. [20] reported a series of cordierite supported V_2O_5–MoO_3/TiO_2 catalysts that were synthesized through an impregnation method for NH_3-SCR. Liu et al. [21] prepared a Al_2O_3-coated cordierite supported CuO catalyst for NH_3-SCR and reported that the SCR reaction followed the E–R mechanism over the synthesized catalyst. In most works, the cordierite ceramics used are commercial products [19–22], which are expensive due to the high fabrication costs and the complex preparation process [23]. In our previous work, porous cordierite ceramics have been successfully synthesized from fly ash and natural minerals. After being carefully characterized, we deduce that they are promising candidates to be catalyst supports [24]. Noticeably, the adoption of SPCC from fly ash helps not only to reduce costs, but also to provide new ways to consume industrial solid waste. Thus, the combination of CeO_2 and SPCC may serve as a potential catalyst for the purification of NO_x at low temperature.

In this study, a series of CPCC supported CeO_x catalysts (Ce/CPCC) with precursors of different concentrations were first prepared via the hydrothermal method, and then the NO_x conversion ratios of the prepared catalysts were evaluated. Thus, the optimal concentration of the precursor could be obtained and then adopted to fabricate CeO_x on SPCC (Ce/SPCC) under the same condition. The SCR activity of Ce/SPCC was then measured and compared with the Ce/CPCC. In order to fully clarify the differences between Ce/CPCC and Ce/SPCC, XRD, BET, SEM, EDS, H_2-TPR and XPS analyses were conducted. In addition, in situ DRIFTS studies were employed to compare the adsorption species of ammonia and nitrogen oxides on the surfaces of both catalysts. Then, the effects of temperature were examined. On the basis of the obtained results, the denitration mechanism of Ce/SPCC was discussed as well.

2. Results and Discussion

2.1. The NH_3-SCR Activity

The optimum concentration of precursor ($Ce(NO_3)_3$) was firstly investigated with CPCC supported samples, varying from 0.05 mol/L to 0.8 mol/L, with the samples denoted as 0.05Ce/CPCC, 0.2Ce/CPCC, 0.4Ce/CPCC, 0.6Ce/CPCC, and 0.8Ce/CPCC separately. The NH_3-SCR activities of the as-prepared samples were evaluated as a function of temperature, as shown in Figure 1a. It is obvious that the prepared CPCC catalysts exhibit preferable NO_x conversion ratios at a high temperature range (>300 °C), and efficiencies greater than 90% are yielded at 300–350 °C for the 0.4Ce/CPCC, 0.6Ce/CPCC, and 0.8Ce/CPCC samples. Meanwhile, with the increment of precursor concentrations, the activities of CPCC catalysts present an initial increasing and then a decreasing trend. Generally, 0.6Ce/CPCC shows the best performance, which could be ascribed to adequate catalytic active sites and a high

specific surface area. If the concentration of the precursor is lower than 0.6 mol/L, there won't be enough catalytic active species and if the concentration is higher, it will lead to the closure of the pores. Therefore, the optimum $Ce(NO_3)_3$ concentration to fabricate the catalyst was determined to be 0.6 mol/L. Then, 0.6 mol/L $Ce(NO_3)_3$ aqueous solution was employed in the fabrication of the SPCC supported catalyst and denoted as 0.6Ce/SPCC. From Figure 1b, the NO_x conversion ratios of 0.6Ce/SPCC firstly increase along with the increased temperature and then diminish when the temperature is higher than 300 °C, achieving over 90% at 250–300 °C. In addition, the N_2 selectivity of 0.6Ce/SPCC remains over 95% throughout the whole testing temperature range, and it can reach as high as 99% at 250–300 °C, indicating that the final products of the SCR reactions are mainly N_2. It is notewothy that 0.6Ce/CPCC can only achieve a 72% NO_x conversion ratio at 250 °C. Hence, Ce/SPCC exhibits a better performance than the Ce/CPCC in NH_3-SCR activity at a low-temperature range. Moreover, the decrease of NO_x conversion ratios of all samples at a high-temperature range could be ascribed to the oxidation of NH_3 into NO_x [25].

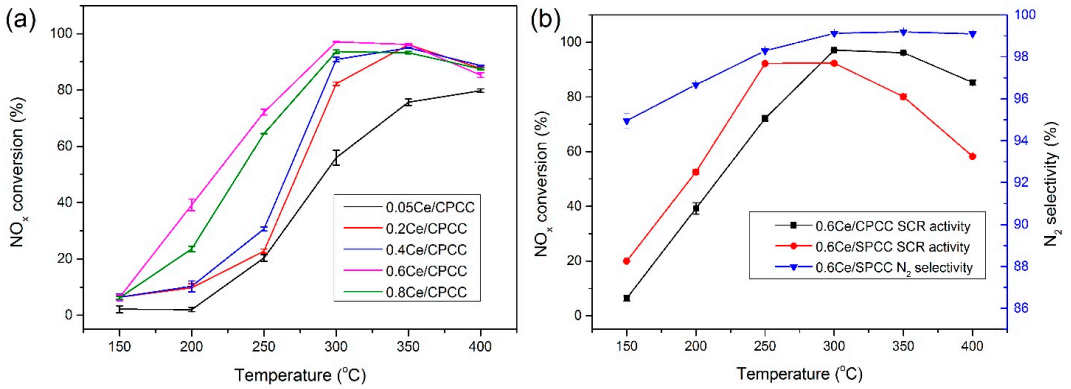

Figure 1. Selective catalytic reduction of NO_x with ammonia (NH_3-SCR) performance of the samples with the variation of temperature. (**a**) CPCC supported samples; (**b**) comparison between 0.6Ce/CPCC and 0.6Ce/SPCC.

2.2. Materials Characterization

2.2.1. SEM Analysis

The morphologies of the supports and the catalyst composites are presented in Figure 2. From Figure 2a,b, the surface of CPCC is more smooth than that of SPCC. The pores of CPCC are mostly small and shallow ones, whereas the pores of SPCC are large and deep ones. After loading CeO_x, as shown in Figure 2c,d, it can be observed that CeO_x particles grow close to each other and hence generate a thin layer on the surface of CPCC. However, CeO_x particles are not evenly distributed. Most particles are observed in the pores of the CPCC support, while few of them can be found on the surface of the CPCC matrix. Figure 2e shows the EDS results of the circled region in Figure 2d and the atom ratio of Ce is 5.1%, which provides evidence for the successful synthesis of CeO_x particles on the supports. The existence of Al, Mg and Si is due to the chemical composition of cordierite ceramics. Nevertheless, a uniform distribution of CeO_x particles could be found on SPCC supports as depicted in Figure 2f,g. Most CeO_x particles on SPCC are less than 500 nm in diameter, and only a few of them are with a diameter of around 1 μm. The EDS mapping results in Figure 2h also reveal that the element Ce is evenly distributed on the surface of the 0.6Ce/SPCC catalyst. Moreover, Ca, Fe and Ti could be detected due to the impurities in fly ash, all of which are also evenly distributed. As demonstrated in our previous work, CaO, Fe_2O_3 and TiO_2 are all components of fly ash based on the XRF results [24]. However, the XRD results (see Figure S1) of both 0.6Ce/CPCC and 0.6Ce/SPCC only show typical peaks for cordierite with no observation of CeO_x, which is mainly attributed to the amount of CeO_x loaded being too low to be detected. Moreover, the textural properties of the samples were characterized and the results (see Table S1) show that the BET surface area of 0.6Ce/SPCC (10.91 m^2/g) is higher than that

of 0.6Ce/CPCC (5.29 m^2/g). Both the morphology and textural analyses show that CeO_x particles have been successfully prepared on the cordierite ceramics supports, but also that a better dispersion of CeO_x active sites can be achieved on the SPCC support, which could be attributed to the impurities that originated from the fly ash, since these impurities provide evenly distributed attachment sites for CeO_x particles to grow on. The good dispersion of CeO_x particles further implies that the catalyst can provide enough active sites to adsorb the reactant species and thus is significant in facilitating catalytic reactions.

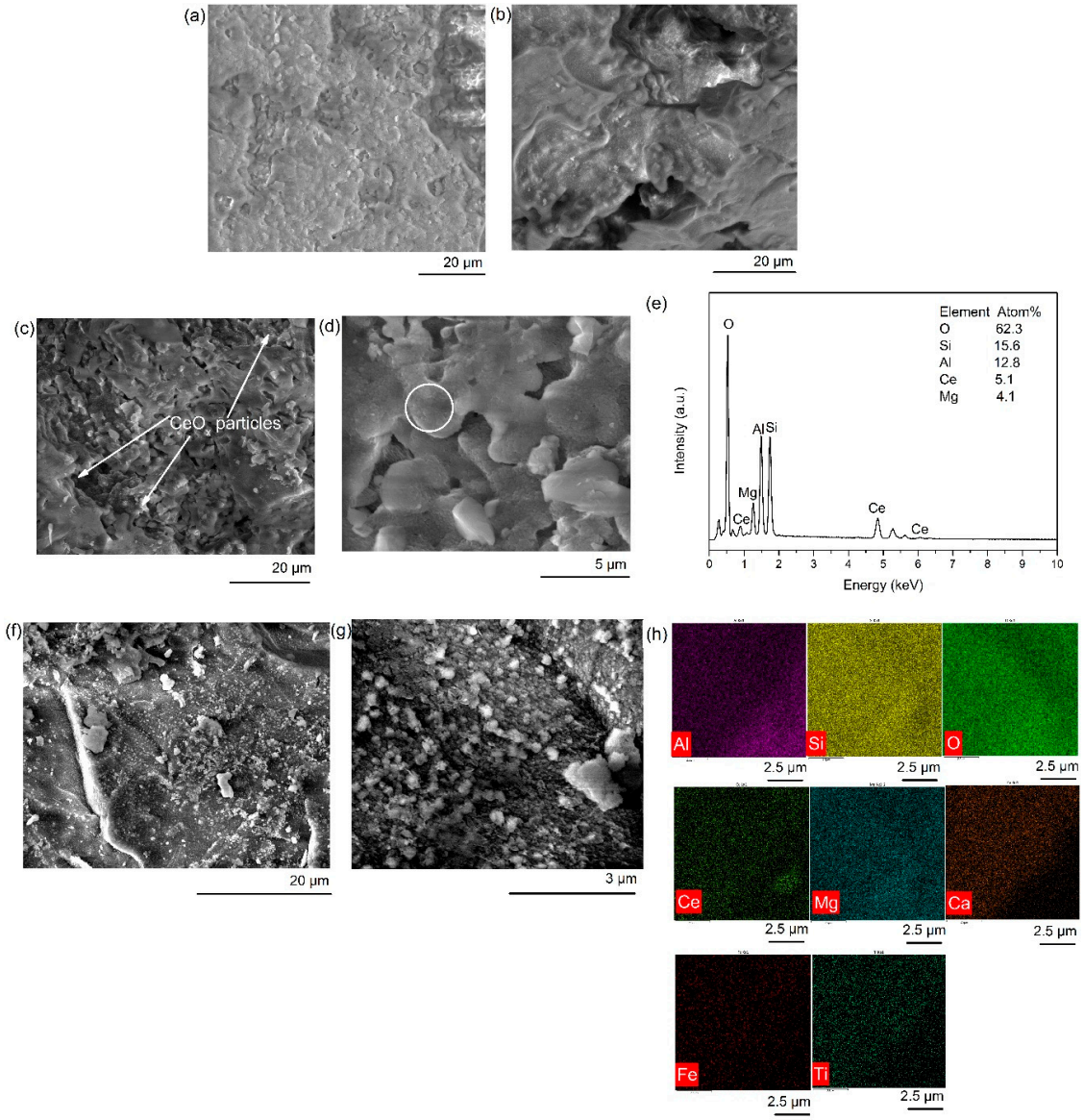

Figure 2. SEM analysis. (**a**) CPCC; (**b**) SPCC; (**c**) 0.6Ce/CPCC; (**d**) magnified image of CeO_x particles of 0.6Ce/CPCC; (**e**) EDS analysis of the circled region in picture (**d**); (**f**) 0. 6Ce/SPCC; (**g**) magnified image of CeO_x particles of 0.6Ce/SPCC; (**h**) EDS mapping of picture (**g**).

2.2.2. Reducibility (H_2-TPR)

The reducibility of the catalysts 0.6Ce/CPCC and 0.6Ce/SPCC were compared by means of H_2-TPR, as presented in Figure 3. Two broad reduction peaks can be found for both of them. The peaks (α and α_1) located at 300–400 °C can be ascribed to the reduction of surface CeO_2 and the peaks (β and β_1) at 650–750 °C represent the bulk CeO_2 reduction, the former of which is normally regarded as being related to the NH_3-SCR activity at a low temperature range [26]. Notably, the peak α of 0.6Ce/SPCC

locates at a lower temperature than α_1 of 0.6Ce/CPCC, which means that the reduction temperature becomes lower when SPCC is adopted. Moreover, the peak area of α is obviously larger than that of α_1. All these features indicate that there are more reducible species on the surface of 0.6Ce/SPCC and that the oxygen storage capacity is enhanced with the adoption of SPCC as the catalyst support [27]. The improvement in reducibility of the SPCC supported sample contributes to the accomplishment of the whole redox process of SCR activities, resulting in better NO_x conversion performance at a lower temperature.

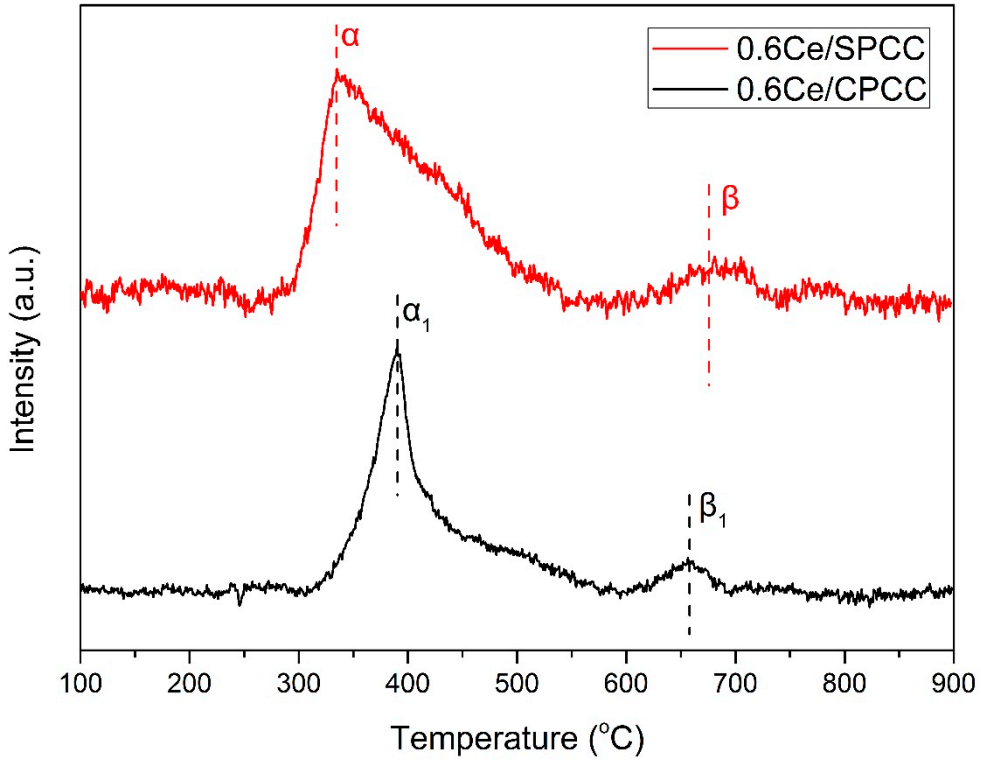

Figure 3. H_2-TPR profiles of the samples.

2.2.3. XPS Analysis

Valence states of Ce of 0.6Ce/CPCC and 0.6Ce/SPCC were characterized by XPS and the results are presented in Figure 4a,b, respectively. The peaks labeled as v′ (~884.5 eV) and u′ (~903.7 eV) are attributed to the $3d^{10}4f^1$ state corresponding to Ce^{3+} ions, while the peaks labeled as v (~882.9 eV), v″ (~887.6 eV), v‴ (~898.7 eV), u (~901.4 eV), u″ (~907.0 eV) and u‴ (~917.0 eV) are assigned to $3d^{10}4f^0$ state of Ce^{4+} species [9,25]. The two spectra show that both Ce^{4+} and Ce^{3+} exist in the two samples and the peak labeled u‴ is usually considered to be the characteristic peak for Ce^{4+} [28,29]. The emergence of Ce^{3+} is due to the valence and defect structure of CeO_{2-x}, leading to the generation of oxygen vacancies to satisfy the electrostatic balance [9]. Oxygen vacancies have been verified to be beneficial to adsorb and activate reactant species, which helps to explain the good performance of CeO_x catalysts in SCR reactions [30]. The intensity of peak u‴ of Figure 4b is stronger than that of Figure 4a, indicating that the Ce^{4+} ratio of 0.6Ce/SPCC is higher. After peak fitting and quantification, we find that the Ce^{3+} ratio of 0.6Ce/CPCC (35.23%) is higher than that of 0.6Ce/SPCC (31.23%). Correspondingly, the Ce^{4+} ratio of 0.6Ce/CPCC is lower, which is in agreement with the aforementioned analysis. Even though 0.6Ce/CPCC has more Ce^{3+} species, the atom percentage of Ce of 0.6Ce/SPCC is 6.16% under XPS analysis, which is higher than that of 0.6Ce/CPCC (2.73%). This result indicates that a higher concentration of catalytic active sites could be found on the surface of SPCC supported catalysts. As 0.6Ce/SPCC exhibited better NO_x conversion performance at lower temperature, the Ce atom ratio is deduced to play a more important role in SCR reactions.

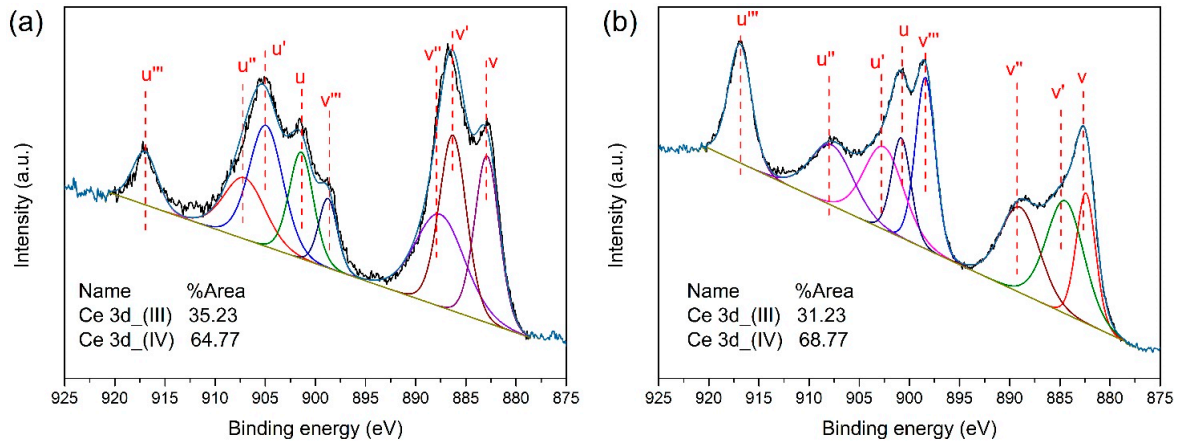

Figure 4. XPS spectra of Ce 3d of 0.6Ce/CPCC (**a**) and 0.6Ce/SPCC (**b**).

2.3. In Situ DRIFTS Studies

2.3.1. Adsorption of NH_3

The DRIFTS spectra of NH_3 adsorption over the samples are presented in Figure 5. In the case of 0.6Ce/CPCC at 150 °C, several bands appeared at 3360, 3278, 1514, 1456 and 1160 cm^{-1} within 2 min. The bands centered at 3360 and 3278 cm^{-1} were progressively strengthened and reached their peaks in 30 min. These two bands were assigned to the NH_3 adsorbed species bonded to Lewis acid sites [31]. The weak band centered at 1160 cm^{-1} which could also be assigned to NH_3 coordinated on Lewis acid sites [32] appeared at first and remained stable for the entire time. The band at 1456 cm^{-1} could be attributed to the NH_4^+ species on Brønsted acid sites [33,34]. The last band at 1514 cm^{-1} could be ascribed to the existence of amide species [34]. From Figure 5b, several bands centered at 3368, 3271, 1580, 1384 and 1295 cm^{-1} could be observed over 0.6Ce/SPCC at 150 °C after NH_3 treatment. Among these bands, the ones located at 3368 and 3271 cm^{-1} could be linked to the adsorbed NH_3 on Lewis acid sites, while the band centered at 1384 cm^{-1} could be ascribed to the NH_4^+ on Brønsted acid sites [34]. The two bands located at 1580 and 1295 cm^{-1} were associated to the $-NH_2$ species [35,36]. Based on the above analysis, both 0.6Ce/CPCC and 0.6Ce/SPCC have Lewis and Brønsted acid sites on the surface. There are more bands related to Lewis acid sites than the Brønsted ones for both of them, indicating that they both have more Lewis acid sites on the surface.

When temperature was increased to 250 °C, the DRIFTS spectra of NH_3 adsorption over 0.6Ce/SPCC were recorded in Figure 5c. Bands at 3332, 3274 and 1166 cm^{-1} were mainly related to NH_3 adsorbed on Lewis acid sites [32]. The band centered at 1583 cm^{-1} indicated the existence of amide species after NH_3 treatment [35]. Two bands located at 965 and 929 cm^{-1} could also be observed, which was mainly due to the weakly adsorbed or gas phase NH_3 [34]. It is noteworthy that there was no band related to Brønsted acid sites that appeared at 250 °C, indicating that the ammonia bonded to Brønsted acid sites is less stable than that on Lewis acid sites [14].

2.3.2. Reaction between Nitrogen Oxides and ad-NH_3 Species

The sample 0.6Ce/SPCC was first exposed to 1000 ppm NH_3 for 30 min, followed by introducing 1000 ppm NO and 3% O_2 to the IR cell. DRIFTS spectra reflecting the reaction process of nitrogen oxides and NH_3 adsorbed species were depicted in Figure 6. As is shown in the figure, coordinated NH_3 on Lewis acid sites (3332, 3274 and 1166 cm^{-1}), weakly adsorbed NH_3 species (965 and 929 cm^{-1}), and $-NH_2$ species (1583 cm^{-1}) all appeared after NH_3 treatment. After the introduction of NO + O_2, the bands at 1166 and 1583 cm^{-1} disappeared immediately, indicating that the NH_3 on Lewis acid sites and the amide species took part in the SCR reaction instantly. The disappearance of the bands 965 and 929 cm^{-1} was due to the reaction between nitrogen oxides and weakly adsorbed NH_3. The bands at high wave numbers (3332 and 3274 cm^{-1}) were gradually weakened, indicating that NH_3 on Lewis

acid sites took part in the SCR reaction for the entire time. In addition, two bands centered at 1527 and 1272 cm^{-1} appeared and became stronger with the accumulation of nitrogen oxides. The band at 1527 cm^{-1} could be ascribed to the formation of monodentate nitrate and the one at 1272 cm^{-1} could be assigned to the linear nitrite species [37,38].

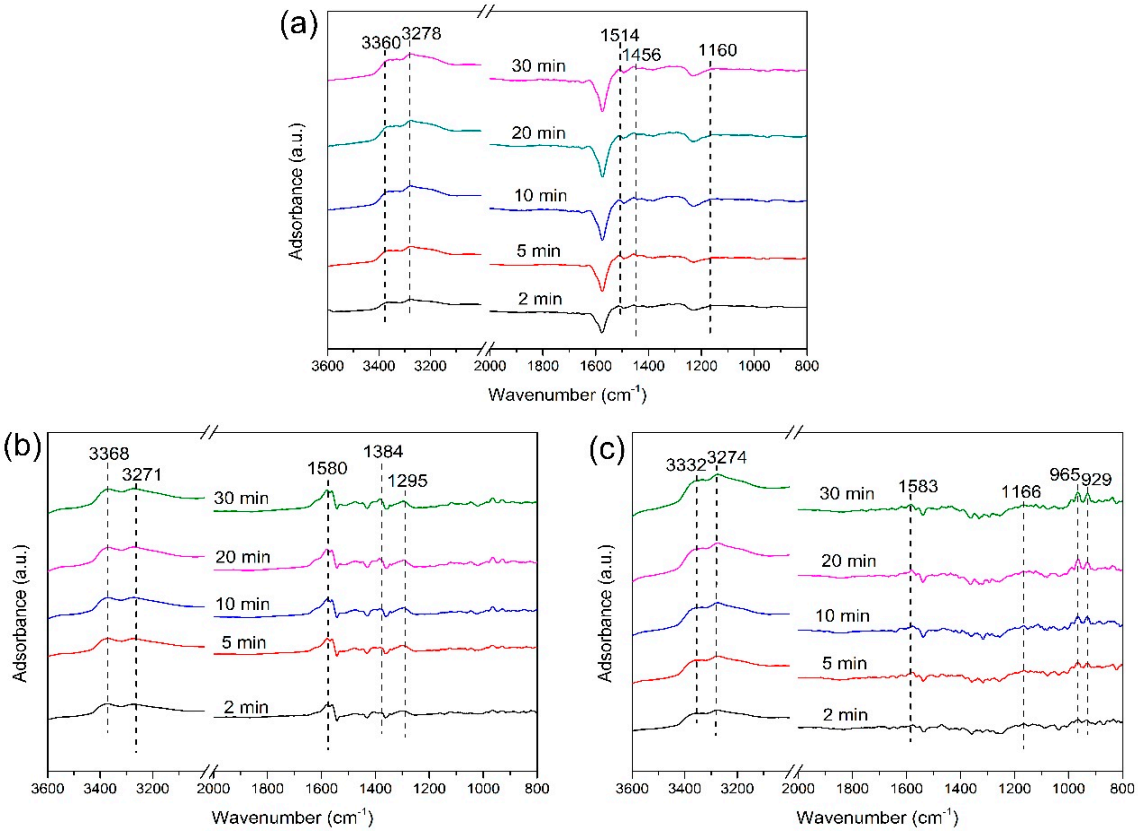

Figure 5. In situ DRIFTS spectra of the samples treated in flowing 1000 ppm NH_3 for 30 min. (**a**) 0.6Ce/CPCC at 150 °C; (**b**) 0.6Ce/SPCC at 150 °C; (**c**) 0.6Ce/SPCC at 250 °C.

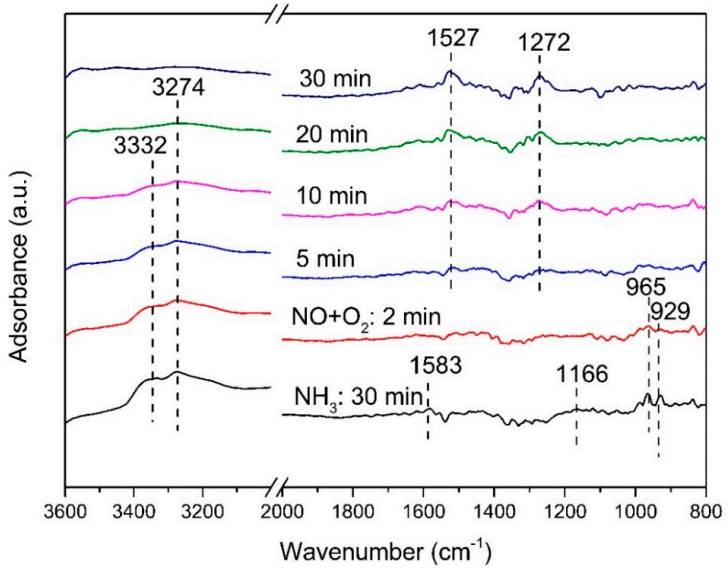

Figure 6. In situ DRIFTS spectra of 0.6Ce/SPCC pretreated with 1000 ppm NH_3 for 30 min followed by exposure to 1000 ppm NO + 3% O_2 at 250 °C for a different period of time.

2.3.3. Co-Adsorption of NO + O_2

The DRIFTS spectra were recorded when the samples were exposed to 1000 ppm NO and 3% O_2 and the results were illustrated in Figure 7. From Figure 7a, two strong bands (1452 and 1281 cm^{-1}) could be detected immediately over 0.6Ce/CPCC at 150 °C, which suggested the formation of monodentate nitrates [38,39]. At 1800–2000 cm^{-1}, two weak bands (1907 and 1842 cm^{-1}) related with weakly adsorbed NO could be identified [10]. However, in the case of 0.6Ce/SPCC at 150 °C, the results were quite different. From Figure 7b, NO adsorbed on oxide surface for covalent bonds (M-N=O, 1696 cm^{-1}) [36,40], NO_2 molecules adsorbed in active state on the surface (1602 cm^{-1}) [9] and nitrite species (1468, 1402 and 1315 cm^{-1}) [38,41] could be observed. The results provide evidence for NO-to-NO_2 conversion. This phenomenon could be ascribed to the promotional effect of the abundant oxygen species over SPCC supported catalysts on the oxidation process of nitrogen oxides. When the temperature is increased to 250 °C, as shown in Figure 7c, the band (1602 cm^{-1}) indicating the NO_2 molecules shifted to 1598 cm^{-1}. Moreover, compared with the 150 °C condition, the number of bands related to the nitrite species (1273 cm^{-1}) [38] was apparently reduced and correspondingly, the number of bands linked with nitrate species (1557, 1528, 1389 and 1295 cm^{-1}) [37,38] was increased. The transition between nitrite and nitrate species was probably due to the high temperature facilitating the oxidation of nitrogen species.

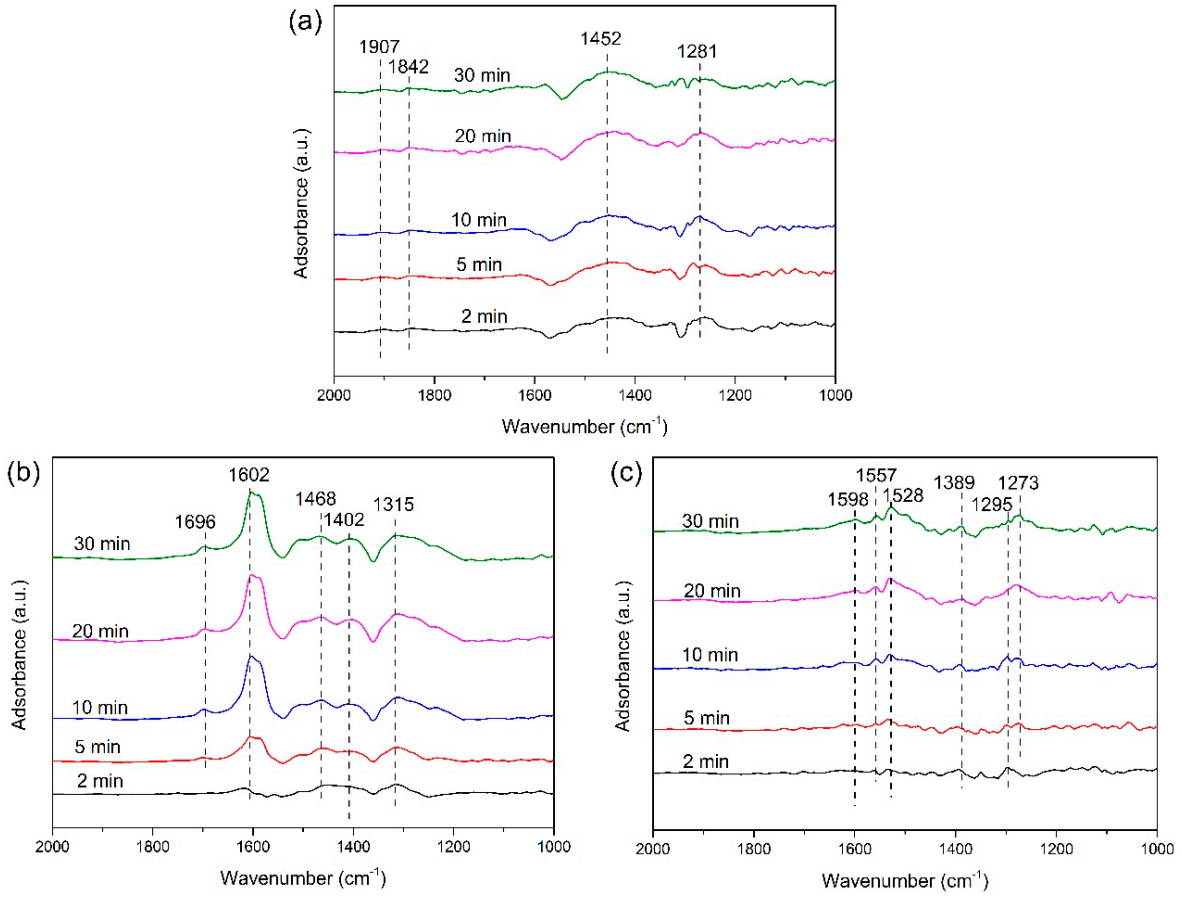

Figure 7. In situ DRIFTS spectra of the samples treated in flowing 1000 ppm NO + 3% O_2 for 30 min. (**a**) 0.6Ce/CPCC at 150 °C; (**b**) 0.6Ce/SPCC at 150 °C; (**c**) 0.6Ce/SPCC at 250 °C.

2.3.4. Reaction between NH_3 and Adsorbed Nitrogen Oxides

In this experiment, 0.6Ce/SPCC was first pretreated by 1000 ppm NO + 3% O_2 for 30 min at 250 °C. Later on, 1000 ppm NH_3 was introduced. The DRIFTS spectra were exhibited in Figure 8. According to the prior analysis, adsorbed NO_2 molecules, nitrite and nitrate species could be detected on the

surface of the sample after being treated in the flow of NO + O_2 for 30 min. From Figure 8, NO_2 species at 1598 cm^{-1} immediately faded away with the admission of NH_3. Nevertheless, all of the nitrite and nitrate species remain unchanged. As for the adsorbed NH_3 species, NH_3 coordinated on Lewis acid sites appeared at 3366 and 3276 cm^{-1}. Moreover, two bands at 966 and 930 cm^{-1} assigned to weakly adsorbed or gaseous NH_3 emerged. Based on the DRIFTS results, it can be deduced that NO_2 was actively involved in the SCR reactions. As is widely acknowledged, the existence of NO_2 greatly facilitates the SCR reaction due to a different reaction path called the "fast SCR reaction" [9]. These results also provide evidence that the two types of adsorbed species (nitrites/nitrates and ad-NH_3) share different adsorption sites on the catalyst surface.

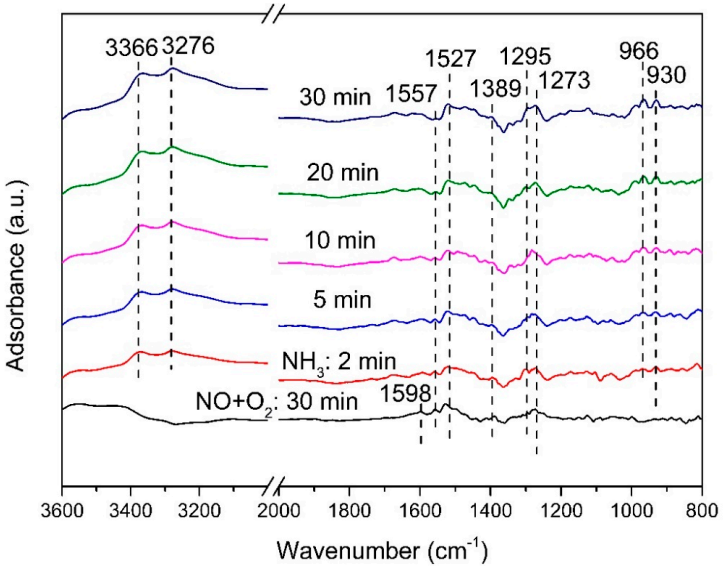

Figure 8. In situ DRIFTS spectra of 0.6Ce/SPCC pretreated with 1000 ppm NO + 3% O_2 for 30 min followed by exposure to 1000 ppm NH_3 at 250 °C for different time.

2.4. Denitration Mechanism of the 0.6Ce/SPCC Catalyst

According to the aforementioned DRIFTS analysis, NH_3 species were easily adsorbed on the catalyst surface. At 250 °C, Lewis acid sites played the dominant role in adsorbing NH_3. With the introduction of NO+O_2, all ad-NH_3 species disappeared with the variation of the time. It is reasonable to deduce that SCR reactions can take place between adsorbed NH_3 and gaseous NO, which follows the E-R route. As for the measurements of the reactions between flowing NH_3 and adsorbed nitrogen species, coordinated NH_3 on Lewis acid sites appeared and the adsorbed NO_2 molecules faded away immediately. Therefore, SCR reactions are estimated to happen between adsorbed NH_3 and adsorbed NO_2 as well, which follows the L-H mechanism. The simplified reactions for the reduction of NO_x to N_2 could be deduced as follows [42,43]:

1. E-R mechanism:

$$NH_3(g) + * \rightarrow NH_3 - * \quad (1)$$

$$O_2(g) + 2* \rightarrow 2O - * \quad (2)$$

$$NH_3 - * + O - * \rightarrow NH_2 - * + OH - * \quad (3)$$

$$NH_2 - * + NO(g) \rightarrow NH_2NO - * \quad (4)$$

$$NH_2NO - * \rightarrow N_2(g) + H_2O \quad (5)$$

2. L-H mechanism:

$$2NO(g) + 2* + O_2(g) \rightarrow 2NO_2 - * \quad (6)$$

$$NH_3(g) + * \rightarrow NH_3 - * \quad (7)$$

$$NO(g) + 2\,NH_3 - * + NO_2 - * \rightarrow 2N_2(g) + 3H_2O \quad (8)$$

(*: active sites on the catalyst surface)

It is noteworthy that the real mechanism is far more complicated than the above analysis and more research efforts should be devoted to this field.

3. Materials and Methods

3.1. Materials

All chemicals were of analytical reagent grade (Beijing Chemical Co., Ltd., China, purity ≥ 99.0%) and were used without any further purification. The catalyst supports were commercial porous cordierite ceramics products from the Corning Company and synthesized porous cordierite ceramics prepared from fly ash (Shuozhou, Shanxi, China), quartz (Shuozhou, Shanxi, China) and magnesite (Haicheng, Liaoning, China) using the method described in our previous work [24]. Briefly, fly ash, quartz and magnesite are mixed together to achieve the stoichiometric content of cordierite. The mixture is then pressed into cylindrical pellets and then sintered at 1300 °C for 2 h. In this way, single-phase porous cordierite can be successfully synthesized.

3.2. Catalyst Preparation

A number of studies have been done to successfully synthesize cerium oxides via different methods. In this study, the hydrothermal method was adopted to prepare the catalyst composites. During the process, $Ce(NO_3)_3.6H_2O$ was first dissolved into the deionized water to obtain an aqueous $Ce(NO_3)_3$ solution with different concentrations (0.05 mol/L, 0.2 mol/L, 0.4 mol/L, 0.6 mol/L and 0.8 mol/L) as precursors. The hydrothermal synthesis was then performed in autoclaves by immersing 1.0 g of substrates with 30.0 mL $Ce(NO_3)_3$ solution at an optimized temperature of 160 °C for 24 h. After the hydrothermal process, samples were rinsed with deionized water and then dried at 160 °C for 24 h. Details of the preparation parameters are summarized in Table 1.

Table 1. Parameters during the hydrothermal process.

Sample	$Ce(NO_3)_3$ Concentration (mol/L)	Catalyst Support	Temperature (°C)	Time (h)
0.05Ce/CPCC	0.05	CPCC	160	24
0.2Ce/CPCC	0.2	CPCC	160	24
0.4Ce/CPCC	0.4	CPCC	160	24
0.6Ce/CPCC	0.6	CPCC	160	24
0.8Ce/CPCC	0.8	CPCC	160	24
0.6Ce/SPCC	0.6	SPCC	160	24

3.3. Catalyst Characterization

The crystal structures of the catalyst composites and supports were characterized by a powder X-ray diffractometer (D/Max 2500, Rigaku, Tokyo, Japan) with Cu K_α radiation at a scanning speed of 8°/min between 10–60° (see Figure S1). The SEM-EDS analyses of the prepared composites were carried out by an environment scanning electron microscope (ESEM; Quattro S, FEI, OR, USA) coupled with an energy dispersive spectrometer (Ultim Max 100, Oxford Instruments, Oxford, UK). Textural properties of the as-prepared catalyst composites were investigated by a nitrogen adsorption apparatus (ASAP2020, Micromeritics, Norcross, GA, USA) at 77 K (see Figure S2). The samples were outgassed at 120 °C for 4 h under vacuum before the measurement. The specific surface area and average pore diameter were calculated with the Brunauer–Emmett-Teller (BET) theory, while the pore volume was obtained from the N_2 desorption isotherm using Barrett–Joyner–Halenda (BJH) equations [44].

Temperature programmed reduction by hydrogen (H_2-TPR) was carried out on a chemical auto-adsorption apparatus (AutoChem 2920, Micromeritics, Norcross, GA, USA). Before the reduction process, the samples (100 mg) were purged under Ar flow at 200 °C for 1 h and then cooled down to 50 °C. The flow through the sample tube was switched over to 5 vol.% H_2 in an Ar mixture. After stabilizing the base line, TPR was carried out with a heating rate of 5 °C/min to 900 °C. The surface atomic states of the samples were determined by XPS (Axis Ultra Dld, Shimadzu/Kratos, Manchester, UK) with Al K_α radiation (hν = 1486.6 eV) at 150 W [45].

3.4. SCR Activity Measurements

The SCR activity was measured in a fixed-bed quartz reactor (inner diameter 10 mm) at temperatures ranging from 150–400 °C at intervals of 50 °C. The relevant data were collected only when the steady state of the reaction was achieved. The typical composition of reactant gas was as follows: 1000 ppm NO, 1000 ppm NH_3, 3% O_2 and balanced N_2. The total flow rate was controlled at 100 mL/min with 1.5 g of catalysts and the gas hourly space velocity (GHSV) was around 4000 h^{-1} which is achievable under industrial circumstances. Analyses of the concentrations of NO and NO_2 at inlet and outlet were recorded by a flue gas analyzer (Pro 350, Testo, Lenzkirch, Germany), while the concentrations of N_2O and NH_3 were measured by an FT-IR gas analyzer (DX4000, GASMET, Vantaa, Finland). NO_x conversion and N_2 selectivity were calculated as follows, respectively:

$$NO_x \text{ conversion } (\%) = \left(1 - \frac{[NO_x]_{out}}{[NO_x]_{in}}\right) \times 100\% \quad (9)$$

$$N_2 \text{ selectivity } (\%) = \left(1 - \frac{2[N_2O]_{out}}{[NH_3]_{in} + [NO_x]_{in} - [NH_3]_{out} - [NO_x]_{out}}\right) \times 100\% \quad (10)$$

3.5. In Situ DRIFTS Studies

The DRIFTS studies were carried out on a Fourier transform infrared spectrometer (Nicolet 6700) equipped with an in situ Harrick DRIFT cell with a ZnSe window and an MCT detector cooled by liquid nitrogen [10]. The catalysts were placed into the cell and then heated to 300 °C in N_2 with a total flow rate of 90 mL/min for 1 h to remove the adsorbed impurities on the surface of the samples [43]. Before reactants adsorption, the initial spectra were recorded as the background and during the test, this background was automatically subtracted. The DRIFTS spectra were recorded by accumulating 100 scans with a resolution of 4 cm^{-1} [10].

4. Conclusions

In summary, 0.6Ce/SPCC presented better SCR activity than 0.6Ce/CPCC at low temperature. The SEM and EDS characterizations indicated that SPCC greatly improved the dispersion of CeO_x particles due to the evenly distributed attachment sites which originated from the impurities that were contained in SPCC. H_2-TPR analysis showed that there were more reducible species on 0.6Ce/SPCC and the XPS findings indicated that a higher concentration of catalytic active sites could be found on the surface of 0.6Ce/SPCC. Finally, in situ DRIFTS measurements suggested that the SCR reactions over 0.6Ce/SPCC can happen not only between adsorbed NH_3 species and gaseous NO, but also between adsorbed nitrogen oxide species and adsorbed NH_3 species, indicating the existence of both E-R and L-H mechanisms. Therefore, SPCC supported CeO_x catalysts are verified to be promising NH_3-SCR catalysts to substitute for vanadium-containing counterparts in low-temperature industrial applications.

Supplementary Materials: The following are available online at http://www.mdpi.com/2073-4344/9/6/496/s1, Figure S1: XRD results of the catalyst supports and composites, Figure S2: N_2-physisorption isotherms of (a) 0.6Ce/CPCC and (b) 0.6Ce/SPCC, Table S1: Textural data of the supports and the catalyst composites.

Author Contributions: Conceptualization, S.W. and X.W.; formal analysis, S.W., Z.Y., Z.C. and B.H.; Writing—Original Draft preparation, S.W.; Writing—Review and Editing, S.W., H.W., L.L., Y.Z. and X.W.; supervision, X.W.; project administration, L.L.; funding acquisition, X.W., L.L. and Z.Y.

Funding: This research was funded by the National Natural Science Foundation of China, grant number 51672006, 51472006 and 51608333. This research was also funded by the Ministry of Land and Resources Public Welfare Industry Research Project (201511062-02).

Conflicts of Interest: The authors declare no conflict of interest.

References

1. Zhao, B.; Wang, S.; Liu, H.; Xu, J.; Fu, K.; Klimont, Z.; Hao, J.; He, K.; Cofala, J.; Amann, M. NO_x emissions in China: historical trends and future perspectives. *Atmos. Chem. Phys.* **2013**, *13*, 9869–9897. [CrossRef]
2. Xie, Z.; Zhou, X.; Wu, H.; Chen, L.; Zhao, H.; Liu, Y.; Pan, L.; Chen, H. One-pot hydrothermal synthesis of CuBi co-doped mesoporous zeolite Beta for the removal of NO_x by selective catalytic reduction with ammonia. *Sci. Rep.* **2016**, *6*, 30132. [CrossRef] [PubMed]
3. Wu, J.; Gong, Z.; Lu, C.; Niu, S.; Ding, K.; Xu, L.; Zhang, K. Preparation and Performance of Modified Red Mud-Based Catalysts for Selective Catalytic Reduction of NO_x with NH_3. *Catalysts* **2018**, *8*, 35. [CrossRef]
4. Paolucci, C.; Khurana, I.; Parekh, A.A.; Li, S.; Shih, A.J.; Li, H.; Di Iorio, J.R.; Albarracin-Caballero, J.D.; Yezerets, A.; Miller, J.T. Dynamic multinuclear sites formed by mobilized copper ions in NO_x selective catalytic reduction. *Science* **2017**, *357*, 898–903. [CrossRef]
5. Topsøe, N.-Y. Mechanism of the selective catalytic reduction of nitric oxide by ammonia elucidated by in situ on-line Fourier transform infrared spectroscopy. *Science* **1994**, *265*, 1217–1219. [CrossRef] [PubMed]
6. Kim, M.; Yang, K. The role of Fe_2O_3 species in depressing the formation of N_2O in the selective reduction of NO by NH_3 over V_2O_5/TiO_2-based catalysts. *Catalysts* **2018**, *8*, 134.
7. Wu, R.; Zhang, N.; Li, L.; He, H.; Song, L.; Qiu, W. DRIFT Study on Promotion Effect of the Keggin Structure over V_2O_5-MoO_3/TiO_2 Catalysts for Low Temperature NH_3-SCR Reaction. *Catalysts* **2018**, *8*, 143. [CrossRef]
8. Xu, L.; Li, X.-S.; Crocker, M.; Zhang, Z.-S.; Zhu, A.-M.; Shi, C. A study of the mechanism of low-temperature SCR of NO with NH_3 on MnO_x/CeO_2. *J. Mol. Catal. A-Chem.* **2013**, *378*, 82–90. [CrossRef]
9. Wang, J.; Yan, Z.; Liu, L.; Zhang, Y.; Zhang, Z.; Wang, X. Low-temperature SCR of NO with NH_3 over activated semi-coke composite-supported rare earth oxides. *Appl. Surf. Sci.* **2014**, *309*, 1–10. [CrossRef]
10. Chen, Y.; Zhang, Z.; Liu, L.; Mi, L.; Wang, X. In situ DRIFTS studies on MnO_x nanowires supported by activated semi-coke for low temperature selective catalytic reduction of NO_x with NH_3. *Appl. Surf. Sci.* **2016**, *366*, 139–147. [CrossRef]
11. Zhao, W.; Li, Z.; Wang, Y.; Fan, R.; Zhang, C.; Wang, Y.; Guo, X.; Wang, R.; Zhang, S. Ce and Zr Modified WO_3-TiO_2 Catalysts for Selective Catalytic Reduction of NO_x by NH_3. *Catalysts* **2018**, *8*, 375. [CrossRef]
12. Shan, W.; Liu, F.; He, H.; Shi, X.; Zhang, C. Novel cerium–tungsten mixed oxide catalyst for the selective catalytic reduction of NO_x with NH_3. *Chem. Commun.* **2011**, *47*, 8046–8048. [CrossRef]
13. Zhou, G.; Zhong, B.; Wang, W.; Guan, X.; Huang, B.; Ye, D.; Wu, H. In situ DRIFTS study of NO reduction by NH_3 over Fe–Ce–Mn/ZSM-5 catalysts. *Catal. Today.* **2011**, *175*, 157–163. [CrossRef]
14. Liu, Z.; Zhang, S.; Li, J.; Ma, L. Promoting effect of MoO_3 on the NO_x reduction by NH_3 over CeO_2/TiO_2 catalyst studied with in situ DRIFTS. *Appl. Catal. B-Environ.* **2014**, *144*, 90–95. [CrossRef]
15. Jiang, D.; Zhang, S.; Zeng, Y.; Wang, P.; Zhong, Q. Active site of O_2 and its improvement mechanism over Ce-Ti catalyst for NH_3-SCR reaction. *Catalysts* **2018**, *8*, 336. [CrossRef]
16. Cao, L.; Chen, L.; Wu, X.; Ran, R.; Xu, T.; Chen, Z.; Weng, D. TRA and DRIFTS studies of the fast SCR reaction over CeO_2/TiO_2 catalyst at low temperatures. *Appl. Catal. A- Gen.* **2018**, *557*, 46–54. [CrossRef]
17. Qu, L.; Li, C.; Zeng, G.; Zhang, M.; Fu, M.; Ma, J.; Zhan, F.; Luo, D. Support modification for improving the performance of MnO_x–CeO_y/γ-Al_2O_3 in selective catalytic reduction of NO by NH_3. *Chem. Eng. J.* **2014**, *242*, 76–85. [CrossRef]
18. Li, P.; Xin, Y.; Li, Q.; Wang, Z.; Zhang, Z.; Zheng, L. Ce–Ti amorphous oxides for selective catalytic reduction of NO with NH_3: confirmation of Ce–O–Ti active sites. *Environ. Sci. Technol.* **2012**, *46*, 9600–9605. [CrossRef]
19. Palma, V.; Barba, D.; Vaiano, V.; Colozzi, M.; Palo, E.; Barbato, L.; Cortese, S.; Miccio, M. Honeycomb Structured Catalysts for H_2 Production via H_2S Oxidative Decomposition. *Catalysts* **2018**, *8*, 488. [CrossRef]

20. Qiu, Y.; Liu, B.; Du, J.; Tang, Q.; Liu, Z.; Liu, R.; Tao, C. The monolithic cordierite supported V_2O_5–MoO_3/TiO_2 catalyst for NH_3-SCR. *Chem. Eng. J.* **2016**, *294*, 264–272. [CrossRef]
21. Liu, Q.; Liu, Z.; Su, J. Al_2O_3-coated cordierite honeycomb supported CuO catalyst for selective catalytic reduction of NO by NH_3: surface properties and reaction mechanism. *Catal. Today.* **2010**, *158*, 370–376. [CrossRef]
22. Su, J.; Liu, Q.; Liu, Z.; Huang, Z. Honeycomb CuO/Al_2O_3/Cordierite Catalyst for Selective Catalytic Reduction of NO by NH_3-Effect of Al_2O_3 Coating. *Ind. Eng. Chem. Res.* **2008**, *47*, 4295–4301. [CrossRef]
23. Liu, C.; Liu, L.; Tan, K.; Zhang, L.; Tang, K.; Shi, X. Fabrication and characterization of porous cordierite ceramics prepared from ferrochromium slag. *Ceram. Int.* **2016**, *42*, 734–742. [CrossRef]
24. Wang, S.; Wang, H.; Chen, Z.; Ji, R.; Liu, L.; Wang, X. Fabrication and characterization of porous cordierite ceramics prepared from fly ash and natural minerals. *Ceram. Int.* **2019**. under review.
25. Zhan, S.; Zhang, H.; Zhang, Y.; Shi, Q.; Li, Y.; Li, X. Efficient NH_3-SCR removal of NO_x with highly ordered mesoporous WO_3 (χ)-CeO_2 at low temperatures. *Appl. Catal. B-Environ.* **2017**, *203*, 199–209. [CrossRef]
26. Yao, X.; Chen, L.; Cao, J.; Yang, F.; Tan, W.; Dong, L. Morphology and Crystal-Plane Effects of CeO_2 on TiO_2/CeO_2 Catalysts during NH_3-SCR Reaction. *Ind. Eng. Chem. Res.* **2018**, *57*, 12407–12419. [CrossRef]
27. Sun, X.; Guo, R.-t.; Liu, S.-w.; Liu, J.; Pan, W.-g.; Shi, X.; Qin, H.; Wang, Z.-y.; Qiu, Z.-z.; Liu, X.-y. The promoted performance of CeO_2 catalyst for NH_3-SCR reaction by NH_3 treatment. *Appl. Surf. Sci.* **2018**, *462*, 187–193. [CrossRef]
28. Vorokhta, M.; Khalakhan, I.; Matolínová, I.; Nováková, J.; Haviar, S.; Lančok, J.; Novotný, M.; Yoshikawa, H.; Matolín, V. PLD prepared nanostructured Pt-CeO_2 thin films containing ionic platinum. *Appl. Surf. Sci.* **2017**, *396*, 278–283. [CrossRef]
29. Nguyen, T.-S.; Postole, G.; Loridant, S.; Bosselet, F.; Burel, L.; Aouine, M.; Massin, L.; Gélin, P.; Morfin, F.; Piccolo, L. Ultrastable iridium–ceria nanopowders synthesized in one step by solution combustion for catalytic hydrogen production. *J. Mater. Chem. A.* **2014**, *2*, 19822–19832. [CrossRef]
30. Jiang, Y.; Bao, C.; Liu, S.; Liang, G.; Lu, M.; Lai, C.; Shi, W.; Ma, S. Enhanced activity of Nb-modified CeO_2/TiO_2 catalyst for the selective catalytic reduction of NO with NH_3. *Aerospl. Air. Qual. Res.* **2018**, *18*, 2121–2130. [CrossRef]
31. Fan, J.; Ning, P.; Song, Z.; Liu, X.; Wang, L.; Wang, J.; Wang, H.; Long, K.; Zhang, Q. Mechanistic aspects of NH_3-SCR reaction over CeO_2/TiO_2-ZrO_2-SO_4^{2-} catalyst: In situ DRIFTS investigation. *Chem. Eng. J.* **2018**, *334*, 855–863. [CrossRef]
32. Jin, R.; Liu, Y.; Wu, Z.; Wang, H.; Gu, T. Low-temperature selective catalytic reduction of NO with NH_3 over MnCe oxides supported on TiO_2 and Al_2O_3: A comparative study. *Chemosphere* **2010**, *78*, 1160–1166. [CrossRef] [PubMed]
33. Larrubia, M.A.; Ramis, G.; Busca, G. An FT-IR study of the adsorption and oxidation of N-containing compounds over Fe_2O_3-TiO_2 SCR catalysts. *Appl. Catal. B-Environ.* **2001**, *30*, 101–110. [CrossRef]
34. Chen, Y.; Wang, J.; Yan, Z.; Liu, L.; Zhang, Z.; Wang, X. Promoting effect of Nd on the reduction of NO with NH_3 over CeO_2 supported by activated semi-coke: an in situ DRIFTS study. *Catal. Sci. Technol.* **2015**, *5*, 2251–2259. [CrossRef]
35. Zhang, Y.; Yue, X.; Huang, T.; Shen, K.; Lu, B. In situ DRIFTS studies of NH_3-SCR mechanism over V_2O_5-CeO_2/TiO_2-ZrO_2 catalysts for selective catalytic reduction of NO_x. *Materials* **2018**, *11*, 1307. [CrossRef]
36. Zhang, Q.; Fan, J.; Ning, P.; Song, Z.; Liu, X.; Wang, L.; Wang, J.; Wang, H.; Long, K. In situ DRIFTS investigation of NH_3-SCR reaction over CeO_2/zirconium phosphate catalyst. *Appl. Surf. Sci.* **2018**, *435*, 1037–1045. [CrossRef]
37. Sazama, P.; Čapek, L.; Drobná, H.; Sobalik, Z.; Dědeček, J.; Arve, K.; Wichterlová, B. Enhancement of decane-SCR-NO_x over Ag/alumina by hydrogen. Reaction kinetics and in situ FTIR and UV–vis study. *J. Catal.* **2005**, *232*, 302–317. [CrossRef]
38. Zhang, R.; Yang, W.; Luo, N.; Li, P.; Lei, Z.; Chen, B. Low-temperature NH_3-SCR of NO by lanthanum manganite perovskites: Effect of A-/B-site substitution and TiO_2/CeO_2 support. *Appl. Catal. B-Environ.* **2014**, *146*, 94–104. [CrossRef]
39. Chen, L.; Si, Z.; Wu, X.; Weng, D. DRIFT study of CuO–CeO_2–TiO_2 mixed oxides for NO_x reduction with NH_3 at Low temperatures. *Acs. Appl. Mater. Inter.* **2014**, *6*, 8134–8145. [CrossRef]

40. Łamacz, A.; Krztoń, A.; Djéga-Mariadassou, G. Study on the selective catalytic reduction of NO with toluene over CuO/$CeZrO_2$. A confirmation for the three-function model of HC-SCR using the temperature programmed methods and in situ DRIFTS. *Appl. Catal. B-Environ.* **2013**, *142*, 268–277. [CrossRef]
41. Wang, W.; McCool, G.; Kapur, N.; Yuan, G.; Shan, B.; Nguyen, M.; Graham, U.M.; Davis, B.H.; Jacobs, G.; Cho, K. Mixed-phase oxide catalyst based on Mn-mullite (Sm, Gd) Mn_2O_5 for NO oxidation in diesel exhaust. *Science* **2012**, *337*, 832–835. [CrossRef]
42. Qi, G.; Yang, R.T. Characterization and FTIR studies of MnO_x−CeO_2 catalyst for low-temperature selective catalytic reduction of NO with NH_3. *J. Phys. Chem. B* **2004**, *108*, 15738–15747. [CrossRef]
43. Wang, J.; Yan, Z.; Liu, L.; Chen, Y.; Zhang, Z.; Wang, X. In situ DRIFTS investigation on the SCR of NO with NH_3 over V_2O_5 catalyst supported by activated semi-coke. *Appl. Surf. Sci.* **2014**, *313*, 660–669. [CrossRef]
44. Zhao, X.; Huang, L.; Li, H.; Hu, H.; Hu, X.; Shi, L.; Zhang, D. Promotional effects of zirconium doped $CeVO_4$ for the low-temperature selective catalytic reduction of NO_x with NH_3. *Appl. Catal. B-Environ.* **2016**, *183*, 269–281. [CrossRef]
45. Jiang, Y.; Bao, C.; Liu, Q.; Liang, G.; Lu, M.; Ma, S. A novel CeO_2-MoO_3-WO_3/TiO_2 catalyst for selective catalytic reduction of NO with NH_3. *Catal. Commun.* **2018**, *103*, 96–100. [CrossRef]